Journal of Applied Electrochemistry **30**: 665–673, 2000.

Impedance spectroscopy and modelling of zinc deposition in chloride electrolyte containing a commercial additive

F. GANNE[1,2], C. CACHET[1*], G. MAURIN[1], R. WIART[1], E. CHAUVEAU[2] and J. PETITJEAN[2]
[1] *Physique des Liquides et Electrochimie, UPR CNRS No. 15 conventionnée avec l'Université de Paris VI, 4 Place Jussieu, 75252 Paris Cedex 05, France*
[2] *LEDEPP Groupe USINOR, 17 Avenue des Tilleuls, 57191 Florange Cedex, France*
*(*author for correspondence, e-mail: cc@ccr.jussieu.fr)*

Received 18 September 1999; accepted in revised form 8 February 2000

Key words: additive, crystal growth, impedance, reaction model, zinc deposition

Abstract

The kinetics of zinc deposition from a concentrated chloride electrolyte containing a commercial additive are investigated by impedance spectroscopy. A reaction model formerly validated for zinc deposition in acidic sulphate medium has been adapted to the present electrolyte and closely related to the elementary steps involved in the crystal growth process. Simulation of the electrode kinetics shows that the additive modifies the deposit morphology by changing some specific rates of the surface steps: slowing down the charge transfer reactions, poisoning the active kink sites and increasing the deposition overpotential. Thus zinc deposition takes place on a surface where the intermediate adions Zn^{+}_{ad} and the active kink sites are more numerous and where the nucleation rate is increased, leading to refined grain size.

1. Introduction

Impedance spectroscopy has already allowed the elaboration of reaction models accounting for the experimental data obtained during zinc electrodeposition from various electrolytes. In alkaline solutions, it has been shown that the discharge of zincate ions, already known to take place in multisteps [1–12], also implies slow processes related to the potential dependencies of the geometrical and electrical properties of a zinc oxide layer present on the electrode surface [13, 14].

In acidic electrolytes, the discharge of Zn^{2+} ions proceeds in two steps coupled by the intermediate adion Zn^{+}_{ad} [15–18]. To explain both the existence of multiple steady-states, revealed by S-shaped current–potential curves, and the presence of three time-constants in the inductive electrode impedance, a reaction model based on the competition between the inhibition by adsorbed hydrogen and the autocatalytic discharge of Zn^{2+} has been developed [19, 20]. In addition the autocatalytic production of adions accelerates the birth of active sites, which can trigger the formation of dendrites at relatively low cathodic overpotential. A simplified version of this model has been shown to be valid for zinc electrodeposition in the highly acidic electrolytes used for zinc electrowinning [21], where steep, but single-valued, current–potential curves have been observed.

Zinc electroplating is performed industrially in very concentrated sulphate or chloride electrolytes, so as to allow the use of high current densities, possibly above 100 A dm^{-2} [22]. Usually small amounts of organic additives are used to improve the homogeneity and the surface state of the zinc deposits. Organic additives in the electrolyte generally modify the current efficiency, change the preferred deposit orientation and increase the overpotential for zinc deposition [23–28]. From impedance spectroscopy, some additives, such as tetrabutylammonium bromide, have been shown to strengthen the inhibiting influence of adsorbed hydrogen and weaken the autocatalytic discharge of Zn^{2+} [27, 28]. Lately, it has been shown that a polyethylene oxide base additive appears to be adsorbed effectively on a electrogalvanized coating in a solution of zinc chloride [35].

The aim of the present work was to study the mechanism of zinc electrodeposition from a concentrated chloride electrolyte ($ZnCl_2$ + KCl) of the type used in industrial lines for the zinc electroplating of steel sheets (US Steel process). By discussing the results of impedance spectroscopy in terms of a reaction model [21] and with the help of the concepts of crystal growth, an attempt will be made to clarify the effect of the additive on zinc deposition.

2. Experimental conditions

Zinc deposits were carried out under galvanostatic conditions using a rotating disc electrode (pure zinc

Goodfellow 99.999%, 5 mm diameter, rotation speed 600 rpm). The reference electrode was Ag/AgCl in 3 M KCl and the counter electrode was a zinc sheet (purity 99.995%).

The solutions were made of 1.6 M $ZnCl_2$ and 5.3 M KCl. They were maintained at 62 °C, at pH 4.7, in an electrolysis cell where the anode and cathode compartments were separated by means of a Nafion® diaphragm (Du Pont). Solution S_1 was additive-free and prepared in the laboratory with Merck products of analytical purity. Solution S_2, already used in the industrial line, contained a small amount of a commercial additive from Atotech. This additive is a liquid containing both a long chain polymer, weakly tensioactive, and a pH-buffer. Solution S_3, prepared in the laboratory, contained the same additive at the volume concentration of 10^{-3}.

In all cases the steady-state polarization curves were corrected for ohmic drop deduced from the high-frequency electrode impedance. The impedance diagrams were recorded for various current densities using a frequency response analyser (Solartron 1250), in the frequency band 60 kHz–10 mHz.

The electroactivity of the additive was studied by cyclic voltammetry (scan rate 5 mV s^{-1}) on a platinum electrode in a blank 1 M KCl electrolyte (pH 5.5). The morphology of deposits, of thickness 10 μm, was investigated by scanning electron microscopy.

3. Experimental results

The influence of the additive on the deposit morphology is illustrated in Figure 1. Without additive, the zinc deposit consisted of coarse grains and large prominences were often observed at the periphery and at the centre of the disc electrode. At high current density, a few dendrites started growing at the electrode periphery.

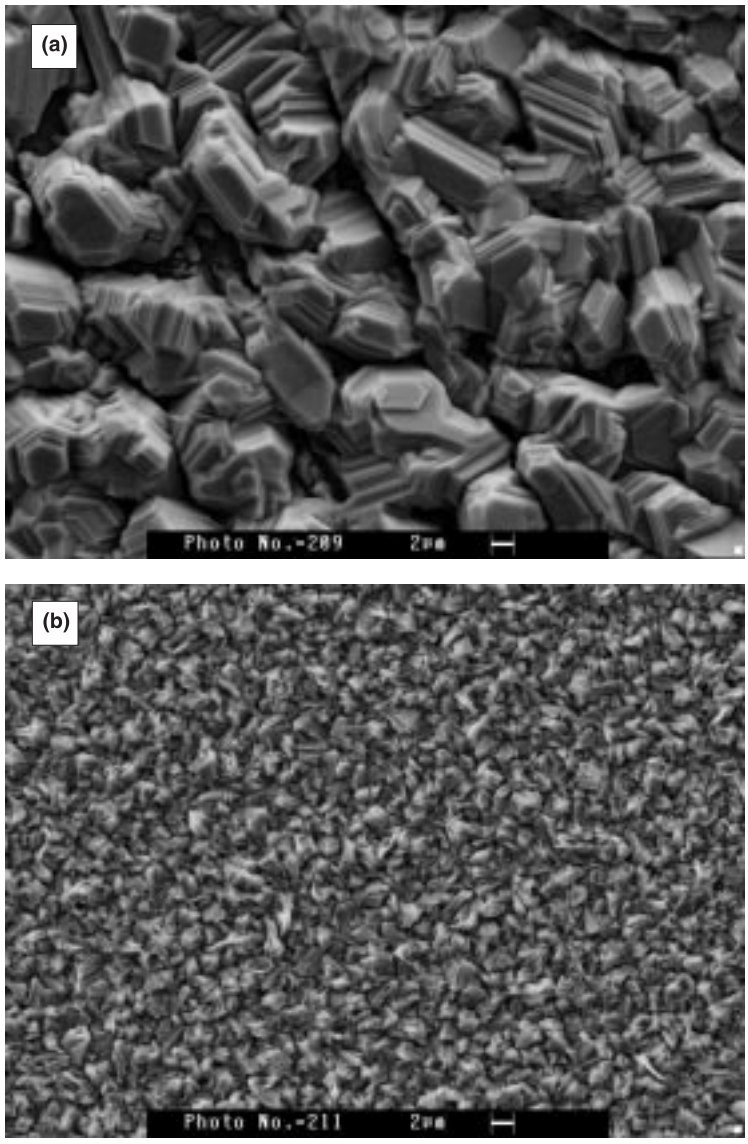

Fig. 1. SEM aspect of zinc deposits of 10 μm thickness realized at 25 mA cm^{-2}: (a) additive-free bath (S_1); (b) with additive at the concentration of 10^{-3} in volume (S_3).

With the additive, the deposit was fine grained and more uniformly distributed on the electrode surface.

In the potential range for zinc electrodeposition, no electroactivity of the additive was detected.

The steady-state polarization curves obtained with the three electrolytes are exhibited in Figure 2. In all cases the rest potential was −1.04 V. With increasing current, the curves become quasi vertical, thus indicating a steep electrode activation. A slight shift in cathodic potential, about 5 mV, appears between curves S_1 and S_2. For solution S_3, more concentrated in additive, the shift is much more pronounced (approximately 35 mV in addition).

Without additive, the complex plane impedance plots were poorly reproducible due to the irregular growth tending to form dendrites. Nevertheless, a medium-frequency capacitive loop and a low-frequency inductive loop were observed, as shown in Figure 3A. The potential drift due to the non steady state of the electrode probably accounts for the untypical behaviour of the low-frequency inductive loop.

With additive, the impedance plots were well reproducible and exhibited, in the low-frequency range, an inductive feature with several time constants: 3 for bath S_2 (Figure 3B and C), 2 for bath S_3 (Figure 3D). The shape of impedance plots was little dependent of current density, except for the separation of time constants which changed in the case of bath S_2.

The resistance R_t corresponding to the size of the high frequency loop can be considered to be the charge transfer resistance. In Figure 4, it appears that the $R_t i$ product can be regarded as current density independent. As compared to the pure electrolyte, the product is increased for bath S_2, and still further for bath S_3, thus indicating that the additive causes inhibition of the charge transfer process. The parameter C_d, deduced from R_t and the frequency at the apex of the high frequency capacitive loop, is not affected by the high-frequency errors caused by the wiring inductance. C_d increases for higher current density where rougher deposits are formed and diminishes in the presence of the additive, as shown in Figure 5, in agreement with the adsorption of organic species. The lowest C_d values correspond to the higher additive concentration in bath S_3.

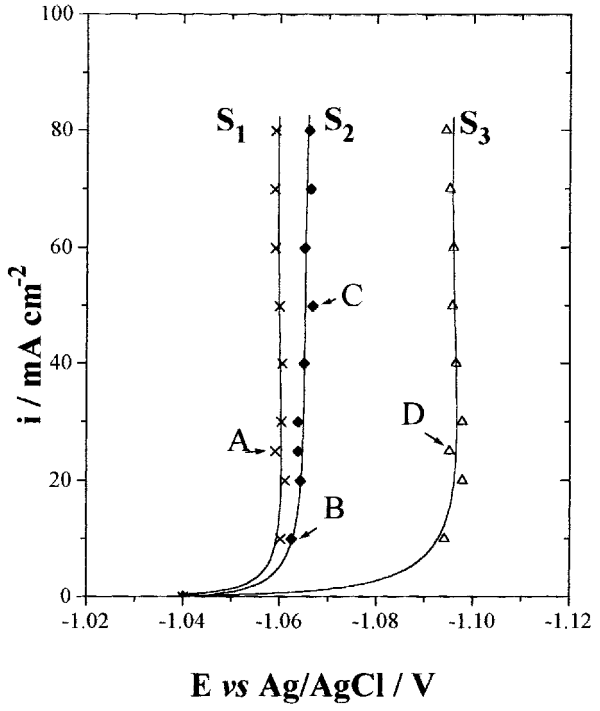

Fig. 2. Experimental steady-state polarization curves for various electrolytes: additive-free bath (S_1); industrial bath (S_2); with additive at the concentration of 10^{-3} in volume (S_3).

4. Reaction model

It is noteworthy that the general shapes of the current–potential curves and impedance plots obtained in concentrated chloride electrolytes are very similar to those previously observed in other acidic electrolytes [19, 20]. Therefore the reaction mechanism for zinc deposition is probably the same, even though different zinc species are present in the electrolytes.

In concentrated chloride electrolytes, analyses of the solutions by Raman spectroscopy has confirmed that zinc is in the form of complex ions $ZnCl_4^{2-}$, in agreement with previous work [29, 30]. This ionic structure was not affected by the presence of the additive. The dissociation step of complex ions was not detected by impedance measurements, thus suggesting that this step is relatively faster than, or not separable from, charge transfer.

The model proposed for a sulfate electrolyte [21] has been adapted to the concentrated chloride electrolyte, the deposition mechanism being considered to occur from Zn^{2+} ions. Starting from the initial set of 11 reactions, the reaction scheme has been simplified by eliminating the steps which accounted for the presence of the oxide/hydroxide adsorbate which was observed in [21] at potentials close to the corrosion potential, but not in the present work. In addition the current–potential curves not being S-shaped, the autocatalytic reaction and the interactions between the adsorbed species H_{ad} and Zn^+_{ad} have been disregarded, for simplicity as in [21]. The final scheme comprising eight reactions is presented in Table 1; the reaction numbering of the previous model [21] has been retained to facilitate the comparison. Close to the corrosion potential, zinc dissolution is considered as the overall Reaction 9, disregarding the elementary steps involved in the mechanism [31].

The first two reactions correspond to the two-step reduction of H^+ ions coupled by the adsorbed intermediate H_{ad}. The discharge of Zn^{2+} ions involves the intermediate adion Zn^+_{ad} and the formation of the active sites Zn^* which act as catalysers in the overall Reaction 11. These sites are permanently renewed on the electrode surface by the slow Reactions 3 and 4.

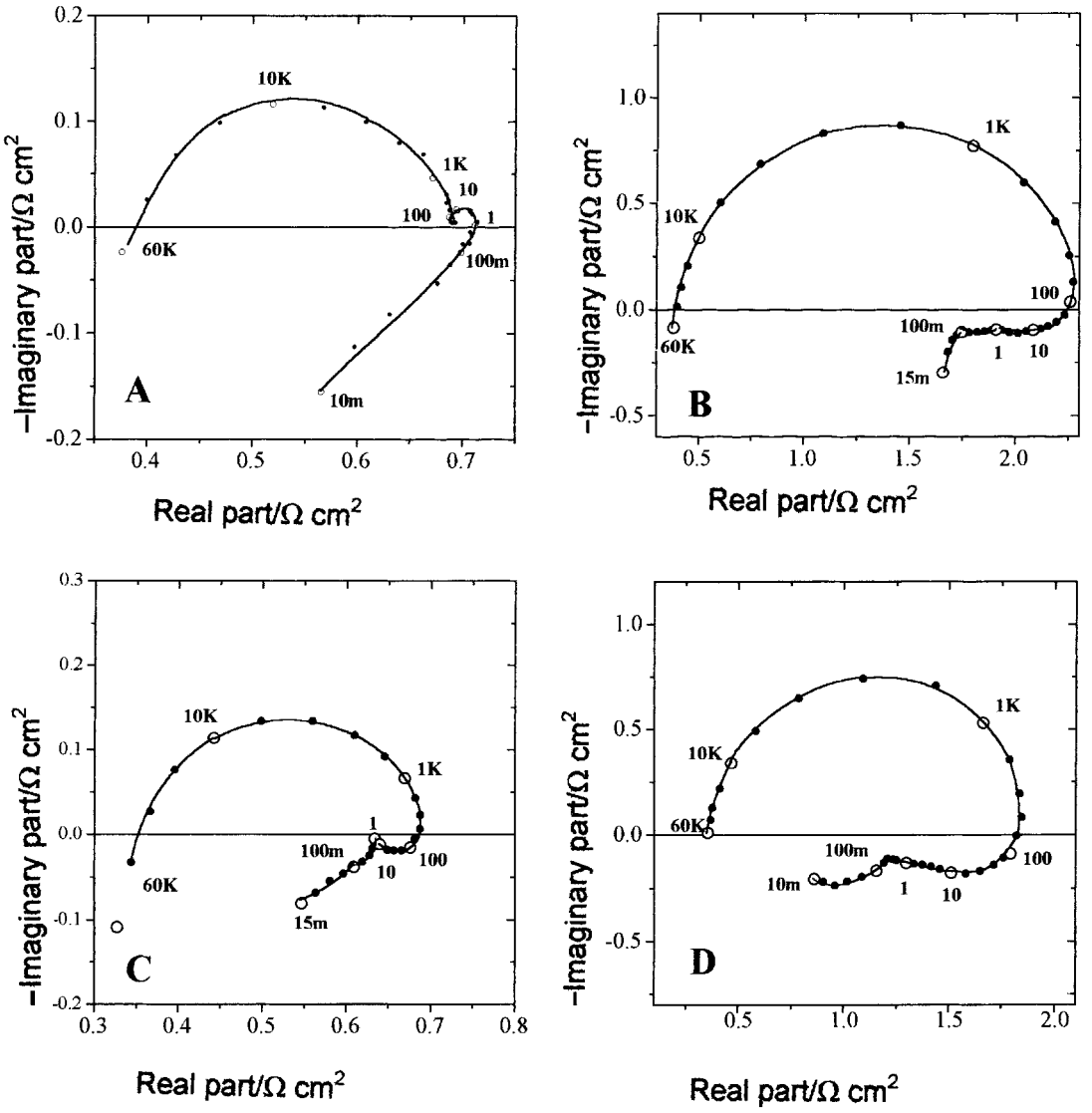

Fig. 3. Complex plane impedance plots measured at points A ($i = 25$ mA cm^{-2}), B ($i = 10$ mA cm^{-2}), C ($i = 50$ mA cm^{-2}) and D ($i = 25$ mA cm^{-2}) in Figure 2. Frequencies in Hz.

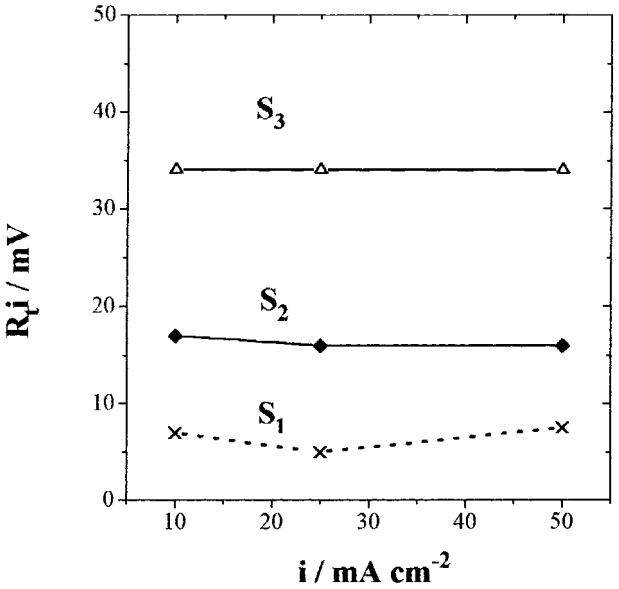

Fig. 4. Experimental current density dependencies of the $R_i i$ product for the three electrolytes.

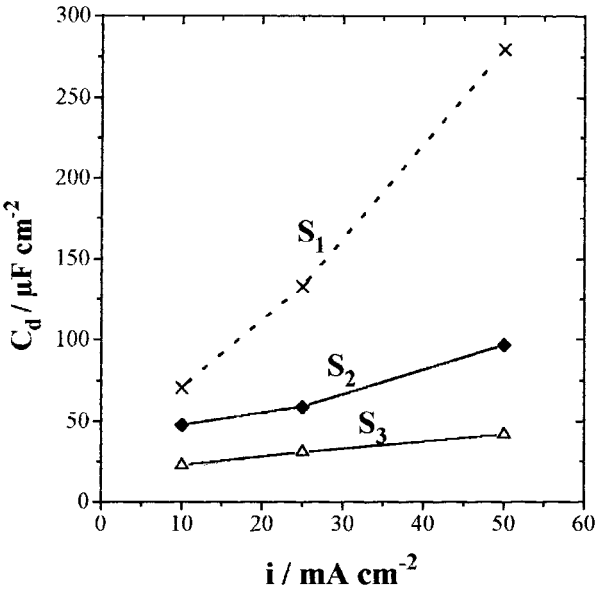

Fig. 5. Current density dependencies of the double layer capacitance for the three electrolytes.

Table 1. Set of reactions considered in the model

$H^+ + e^- \xrightarrow{1} H_{ad}$
$\uparrow$
$H_{ad} + H^+ + e^- \xrightarrow{2} H_2$
$Zn^{2+} + e^- \xrightarrow{6} Zn^+_{ad}$
$Zn^+_{ad} + e^- \xrightarrow{5} Zn$
$Zn^+_{ad} + e^- \xrightarrow{3} Zn^*$
$Zn^* \xrightarrow{4} Zn$
$Zn^{2+} + Zn^* + 2e^- \xrightarrow{11} Zn^* + Zn$
$Zn \xrightarrow{9} Zn^{2+} + 2e^-$

All reactions are coupled by their occurrence on different fractions Θ_i of the electrode surface, due to the electrode coverages by the surface species: H_{ad}, Zn^+_{ad} and Zn^*.

5. Simulation of electrode kinetics

On the basis of the reaction model, polarization curves and complex plane impedance plots have been simulated considering that the adsorption processes follow the Langmuir isotherm, and the rate constants of the electrochemical reactions obey Tafel's law. Each reaction i has a normalized rate constant $A_i = a_i \exp[-b_i(E - E_o)]$, where b_i is the activation coefficient with the cathodic potential E, a_i includes both the rate constant and the concentration of the reacting species, and E_o is an arbitrary chosen origin of potential ($E_o = -1.05$ V). With these assumptions, the material and electron balances have been calculated, as functions of the electrode coverages θ_1, θ_2 and θ_3 by the adsorbed species H_{ad}, Zn^+_{ad} and Zn^*, respectively, as in [21].

The total cathodic current density, i, results from the partial current densities i_{Zn} for zinc deposition, i_C for zinc corrosion and i_H for hydrogen evolution:

$$i = i_{Zn} - i_C + i_H \tag{1}$$

with

$$i_{Zn} = F(A_6(1 - \theta_1 - \theta_2) + A_5\theta_2 + 2A_{11}\theta_3 + A_3\theta_2) \tag{2}$$

in which $FA_3\theta_2$ is the current density i_3 corresponding to the permanent formation of active sites necessary to maintain a steady state, when a permanent poisoning or inclusion of active sites on the deposit surface occurs.

The faradaic impedance, Z_f, given by

$$\frac{1}{Z_f} = \frac{1}{R_t} + \frac{\partial i}{\partial \theta_1}\frac{\Delta\theta_1}{|\Delta E|} + \frac{\partial i}{\partial \theta_2}\frac{\Delta\theta_2}{|\Delta E|} + \frac{\partial i}{\partial \theta_3}\frac{\Delta\theta_3}{|\Delta E|} \tag{3}$$

involves the charge transfer resistance R_t and the relaxation processes of the three electrode coverages. Finally, the total electrode impedance can be calculated considering Z_f in parallel with C_d chosen as the mean values measured with the different electrolytes.

The simulations allow the semi-quantitative reproduction of the experimental results, as shown in Figures 6–8. Sets 1, 2 and 3 of the parameters in Table 2 account for the experimental results obtained with solutions S_1, S_2 and S_3, respectively.

By comparing the three sets of parameters, it appears that the additive slows the charge transfer Reactions 5, 6 and 11 for zinc deposition, particularly by decreasing the activation coefficients b_5, b_6 and b_{11}, in agreement with the increased $R_t i$ product. The decreased values of a_9 in sets 2 and 3 indicate that the additive also inhibits the zinc dissolution process.

According to the present reaction model, the electrode blocking by the adsorbed additive is accounted for in terms of a strengthened adsorption of hydrogen (parameter a_1) and a decreased desorption rate (parameter a_2) but suddenly activated with cathodic potential (increased parameter b_2). This stimulation of the hydrogen adsorption by an additive has already been reported for the tetrabutylammonium bromide [28]. A different description of the electrode blocking by an additive has been proposed using a more complete reaction model considering the existence of oxidized zinc species at potentials close to the corrosion potential: this

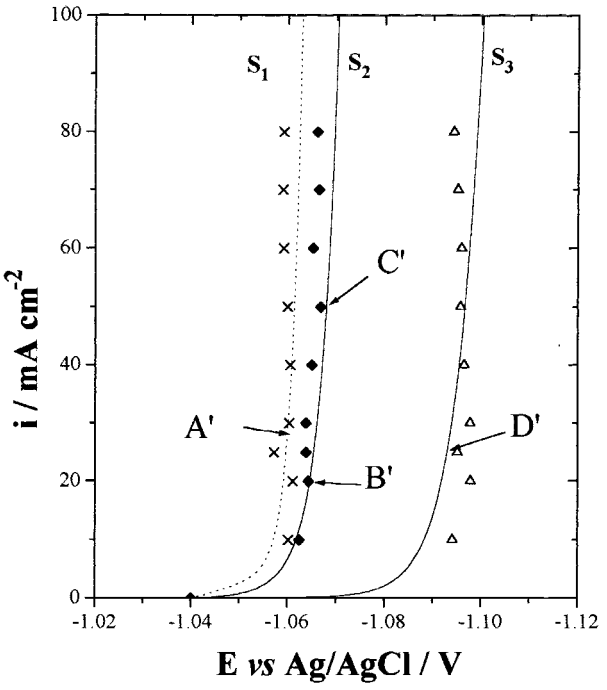

Fig. 6. Steady-state polarization curves calculated with the sets of parameters in Table 2. Experimental points are reported: Key: (curve S_1) set 1; (curve S_2) set 2; (curve S_3) set 3.

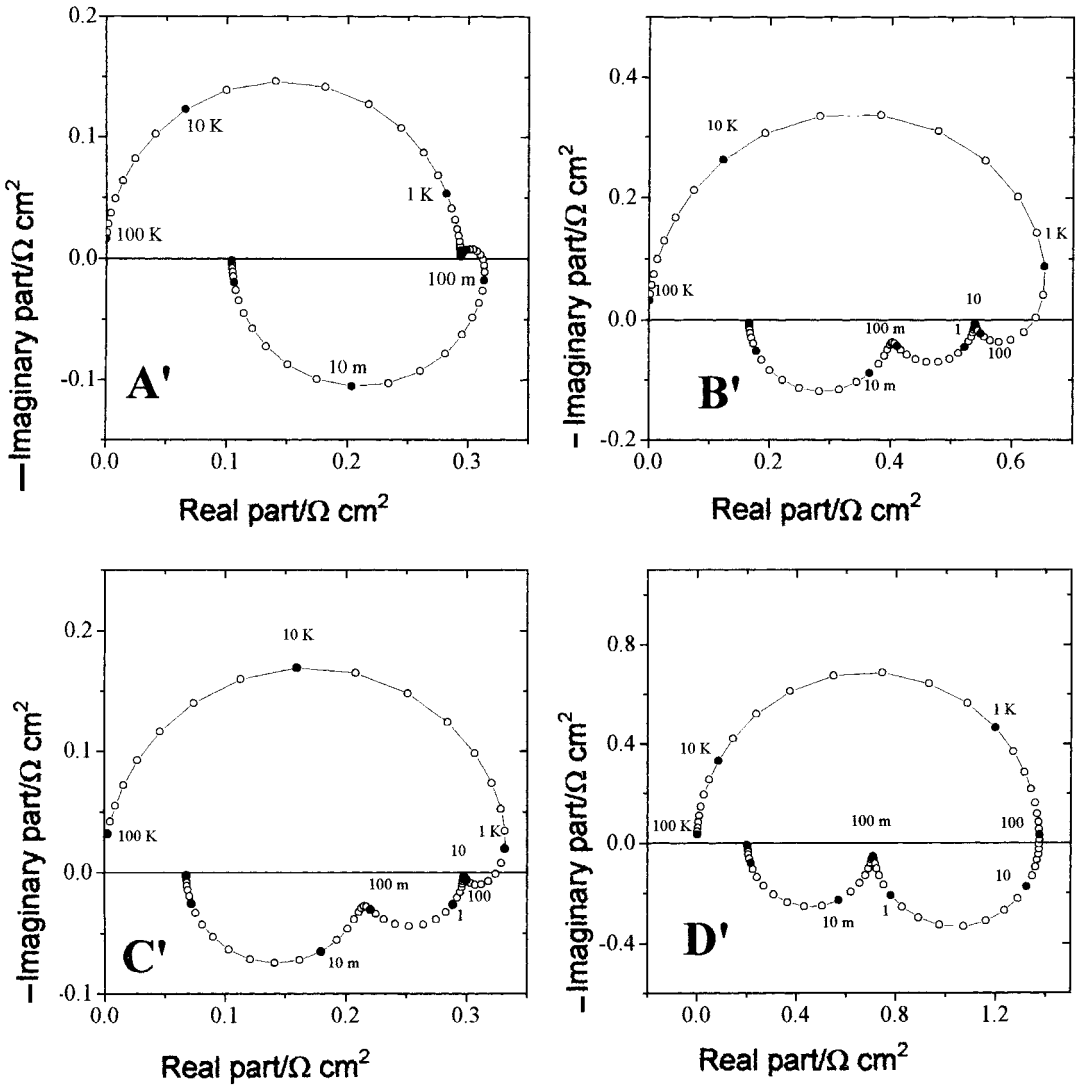

Fig. 7. Complex plane impedance plots calculated at points A′ ($i = 25$ mA cm^{-2}), B′ ($i = 20$ mA cm^{-2}), C′ ($i = 52$ mA cm^{-2}) and D′ ($i = 25$ mA cm^{-2}) in Figure 6. Frequencies in Hz.

situation was prevailing for the perfluorinated surfactant Forafac F1110 which strengthens the adsorption of the oxidized species [34]. Formally, the two possibilities are equivalent to producing an electrode blocking by the adsorbed additive. The modified parameters of Reactions 1 and 2 in sets 2 and 3, and particularly the increased value of a_1 in set 3, cause the two inductive loops, distinguishable in the 100–0.1 Hz frequency range on plots B′ and C′, become a single inductive loop on plot D′, as shown in Figure 7. On the other hand, the strong activation coefficient b_1 in set 1, corresponding to a strongly activated hydrogen adsorption, accounts for the second capacitive loop, at medium frequencies, on plot A′.

In set 3, the changes in parameters b_3 and a_4 mean that the electrode coverage by the active sites Zn^* is also affected by the adsorbed additive, thus reducing the size of the low-frequency inductive loop on plot D′ (Figure 7). Therefore, it appears that the additive inhibits the electrodeposition process by poisoning the active sites Zn^*.

6. Reaction scheme and crystal growth

It is of interest to relate the reaction scheme devoted to the explanation of the results of electrodeposition kinetics to the elementary steps of crystal growth. In terms of crystal growth, Bockris and Razumney [32] and Budevski et al. [33] have attempted to model electrodeposition by considering the kinetics of the elementary steps at the atomic scale and by deducing the overall current in relation with the deposit morphology.

In previous work, the kinetics of the interfacial reactions were related to the deposit morphology [20]. On the one hand, a coupling between the reactions and the surface diffusion of the adions Zn^+_{ad} was shown to be the origin of the spongy deposits which occurred at low current density. On the other hand, a strong acceleration of the nucleation rate, as a result of the autocatalytic formation of the adions, played a major role in the formation of dendrites at high current density. These relations were established considering that the interfa-

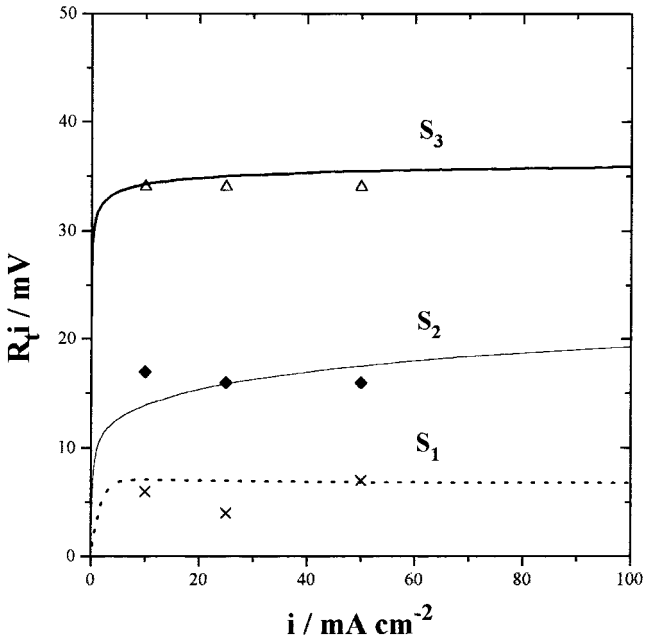

Fig. 8. Simulated current density dependencies of the $R_t i$ product. Experimental points are reported (same conditions as for Figure 6).

cial reactions took place on particular surface sites, assimilating the active sites Zn* to kink sites.

In the present work, this reasoning was pursued to draw a parallel between the various steps of the reaction model in Table 1 and the different crystal growth events.

Table 2. Three sets of parameters used for the simulations

Parameters*	Set 1	Set 2	Set 3
a_1	0.6×10^{-8}	id	0.4×10^{-7}
b_1	40	1	id
a_2	0.1×10^{-8}	0.2×10^{-9}	0.3×10^{-10}
b_2	1	20	110
a_3	0.1×10^{-10}	id	id
b_3	400	160	55
a_4	0.6×10^{-10}	0.3×10^{-10}	id
a_5	0.3×10^{-5}	id	0.3×10^{-6}
b_5	110	20	12
a_6	0.13×10^{-6}	id	0.5×10^{-7}
b_6	100	160	50
a_9	0.7×10^{-8}	0.9×10^{-9}	0.2×10^{-10}
b_9	−40	id	id
a_{11}	0.7×10^{-6}	0.6×10^{-6}	0.14×10^{-6}
b_{11}	150	36	27
C	0.1×10^{-3}	0.5×10^{-4}	0.45×10^{-4}

* (a_i in cm^{-2} s^{-1}; b_i in V^{-1} for reaction i, C in F cm^{-2})

For simplicity, Figure 9 shows the growth of a single crystal which occurs on terraces delimited by edges. The easiest way of incorporating new atoms in the crystal network occurs on the kink sites located on the edges. A competitive way consists in the formation of new nuclei which can be two-dimensional as featured on Figure 9 or three-dimensional, thus generating new grains. The five reactions which account for the reduction of Zn^{2+} ions can be organized in two competitive pathways:

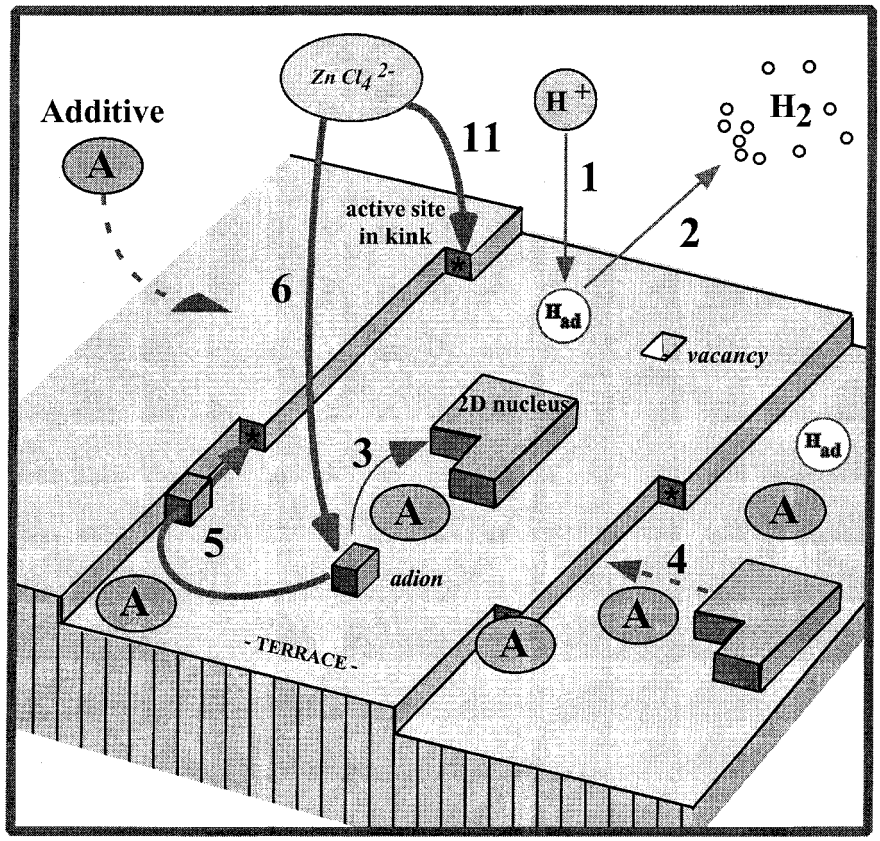

Fig. 9. Scheme for the growth of a single crystal. Representation of the reactions involved in zinc electrocrystallization.

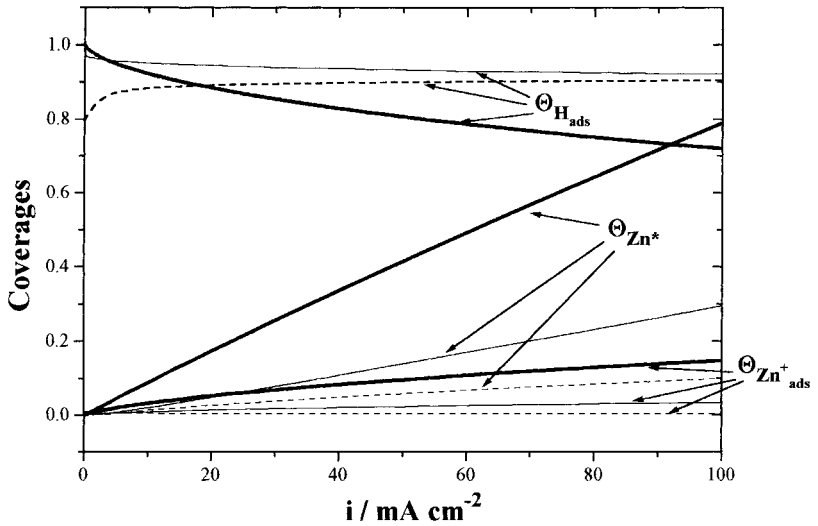

Fig. 10. Current density dependencies of the electrode coverages by H_{ad}, Zn^{+}_{ad} and Zn^{*} calculated with the three sets of parameters in Table 2. Key: (----) S_1; (—) S_2; (▬) S_3.

Path 1. Reduction of Zn^{2+} (or $ZnCl_4^{2-}$) in two steps (Reactions 6 and 5) involving the intermediate adion Zn^{+}_{ad} able to diffuse on the electrode surface. The surface diffusion does not generate a low-frequency capacitive loop, even with additive where this surface step should be hindered by the adsorbed molecules. Consequently it can be considered that surface diffusion is faster than charge transfer, which controls Reaction 5 taking place on the incorporation sites without changing their surface concentration.

Path 2. Direct reduction of Zn^{2+} (or $ZnCl_4^{2-}$) in a single step (Reaction 11) on the active kink sites Zn^{*} whose permanent renewal is ensured by Reactions 3 and 4. Generated, for example, by the formation of 2D or 3D-nuclei, the kink sites Zn^{*} can be either deactivated by the overlap of an edge with a 2D-nucleus, or poisoned by the adsorption of a foreign species, for example, the additive molecules.

All these reactions can be affected by the additive molecules 'A' adsorbed on the electrode surface. As illustrated in Figure 9, the molecules can inhibit the charge transfer Reactions 5, 6 and 11 by blocking different sites on the electrode surface, in particular by poisoning the kink sites Zn^{*}.

The current dependencies of the electrode coverages by the adsorbed species are depicted in Figure 10. In the additive-free solution, the electrode is mainly covered by H_{ad} and the coverages by Zn^{+}_{ad} and Zn^{*} remain very low. In the presence of the additive, especially with solution S_3, increasing current favors the electrode activation with a concomitant increase in the electrode coverages by Zn^{+}_{ad} and Zn^{*}. To obtain a given current density of zinc deposition (galvanostatic mode), the cathodic polarization shift results in increased numbers of both adions and active kink sites, as shown in Figure 10.

It is noteworthy that based on the model, it is possible to express the partial current density i_3 devoted to the

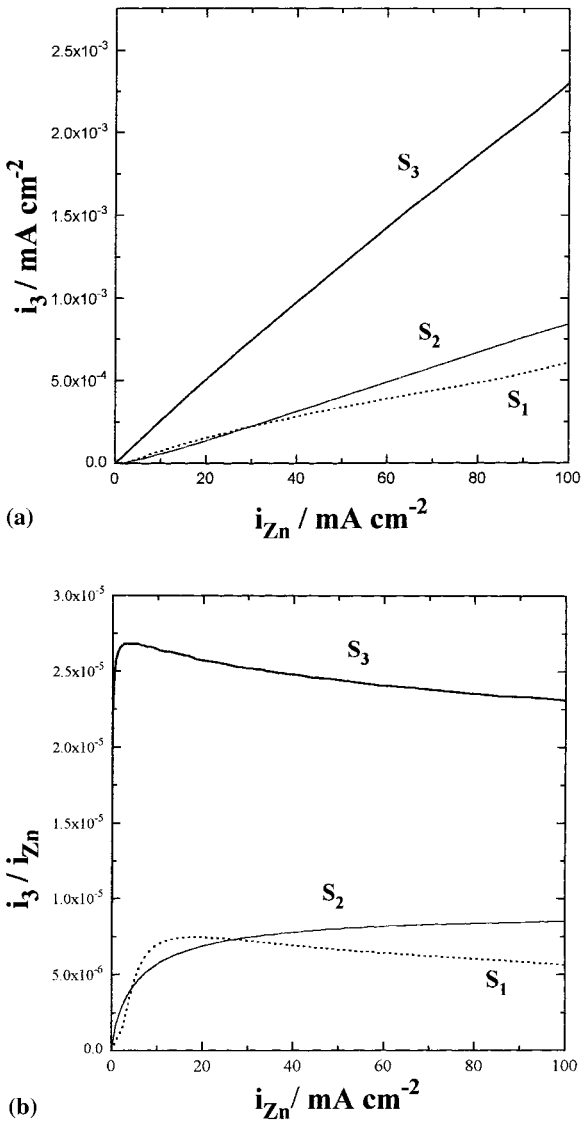

Fig. 11. Current density i_{Zn} dependencies of current density i_3 (a); part of current density i_3 to the current density i_{Zn} (b).

formation of new nuclei. An increase in the nucleation current density i_3 is observed with the additive, mainly for solution S_3 (Figure 11(a)). The part of i_3 to the current density i_{Zn} remains low, as shown in Figure 11(b): the peak appearing at low current density for solutions S_1 and S_3 shows that the contribution of the nucleation is larger at low current density than at high current density. For solution S_2, no peak is observed, and the nucleation rate increases progressively with the current density. These nucleation effects modify the microrelief of deposits by decreasing the length of terraces and producing new nuclei. These two combined effects lead to finer-grained deposits, as shown in Figure 1.

7. Conclusion

The reaction mechanism of zinc deposition in chloride electrolyte containing a commercial additive has been established from impedance spectroscopy analysis. Combining the reaction model with the elementary concepts of crystal growth, the two competitive ways for the crystal growth have been related to the various steps of the reaction model. In particular, it is possible to estimate the partial current density consumed for the birth of new kink sites resulting from a nucleation process.

The simulation of the electrode kinetics observed during zinc deposition highlights the specific influence of the adsorbed additive on the rates of charge transfer reactions and on the elementary steps of crystal growth. The additive strengthens the hydrogen adsorption, slows the charge transfer reactions and poisons the active sites Zn^*. By increasing cathodic polarization, the additive makes zinc deposition occur on a surface covered with more numerous active sites and intermediate adions.

Acknowledgements

The authors thank Mr S. Borensztajn for the SEM investigations of the deposits and Mrs M. C. Bernard and S. Joiret for Raman spectroscopy analysis of the electrolytes.

References

1. N.A. Hampson, G.A. Herdman and R. Taylor, *J. Electroanal. Chem.* **25** (1970) 9.
2. T.P. Dirkse and N.A. Hampson, *Electrochim. Acta* **17** (1972) 135.
3. T.P. Dirkse and N.A. Hampson, *Electrochim. Acta* **17** (1972) 1113.
4. T.P. Dirkse, *J. Electrochem. Soc.* **126** (1979) 541.
5. T.P. Dirkse, *J. Electrochem. Soc.* **126** (1979) 1456.
6. T.P. Dirkse, *J. Electrochem. Soc.* **127** (1980) 1452.
7. J. O'M Bockris, Z. Nagy and A. Damjanovic, *J. Electrochem. Soc.* **119** (1972) 285.
8. J. Hendrickx, A. Van Der Putten, W. Visscher and E. Barendrecht, *Electrochim. Acta* **29** (1984) 81.
9. Y.C. Chang and G. Prentice, *J. Electrochem. Soc.* **131** (1984) 1465.
10. Y.C. Chang and G. Prentice, *J. Electrochem. Soc.* **132** (1985) 375.
11. D.A. Payne and A.J. Bard, *J. Electrochem. Soc.* **119** (1972) 1665.
12. A.R. Despic, D. Jovanovic and T. Rakic, *Electrochim. Acta* **21** (1976) 63.
13. C. Cachet, B. Saïdani and R. Wiart, *Electrochim. Acta* **33** (1988) 405.
14. C. Cachet, B. Saïdani and R. Wiart, *J. Electrochem. Soc.* **138** (1991) 678.
15. L. Gaiser and K.E. Heusler, *Electrochim. Acta* **15** (1970) 161.
16. T. Hurlen and E. Eriksrud, *J. Electroanal. Chem.* **45** (1973) 405.
17. K.E. Heusler and R. Knodler, *Electrochim. Acta* **18** (1973) 855.
18. D.M. Drazic, S. Hadzi-Jordanov and Z. Nagy, *Croat. Chem. Acta* **45** (1973) 199.
19. I. Epelboin, M. Ksouri and R. Wiart, *J. Electrochem. Soc.* **122** (1975) 1206.
20. I. Epelboin, M. Ksouri and R. Wiart, *Faraday Disc. Chem. Soc.* No. 12 (1978) 115.
21. C. Cachet and R. Wiart, *J. Electrochem. Soc.* **141** (1994) 131.
22. A. Weymeersch, R. Winand and L. Renard, *Plat. Surf. Finish.* **68** (1981) 56.
23. M. Sanchez Cruz, F. Alonso and J.M. Palacios, *J. Appl. Electrochem.* **20** (1990) 611.
24. D.J. Mackinnon, R.M. Morrison, J.E. Mouland and P.E. Warren, *J. Appl. Electrochem.* **21** (1991) 213.
25. S.C. Das, P. Singh and G.T. Hefter, *J. Appl. Electrochem.* **26** (1996) 1245.
26. C. Cachet, R. Wiart, I. Ivanov, Y. Stefanov and S. Rashkov, *J. Appl. Electrochem.* **24** (1994) 713.
27. J. Bressan and R. Wiart, *J. Appl. Electrochem.* **7** (1977) 505.
28. J. Bressan and R. Wiart, *J. Appl. Electrochem.* **9** (1979) 43.
29. N.A. Farnsworth and J.S. Gaffney, *Appl. Spectros.* **44** (1990) 469.
30. Z. Kecki, *Spectrochim. Acta* **18** (1962) 1165.
31. C. Cachet and R. Wiart, *J. Electroanal. Chem.* **129** (1981) 103.
32. J. O'M. Bockris and G.A. Razumney, 'Fundamental Aspects of Electrocrystallization' (Plenum Press, New York, 1967).
33. Budevski, G. Staikov and W.J. Lorenz, 'Electrochemical Phase Formation and Formation and Growth' (VCH, Weinheim/New York, 1996).
34. C. Cachet and R. Wiart,*Electrochim. Acta* **44** (1999) 4743.
35. J. Park and H. Kim, *Plat. Surf. Finish.* **86** (1999) 108.